Desalination and Water Treatment
www.deswater.com

doi:10.5004/dwt.2019.24187

160 (2019) 343–353
August

Efficient removal of cationic dyes from aqueous solutions by polydopamine functionalized NH_2-MIL-53(Al)

Si-ying Lin[a], Yin-yin Xu[a,*], Xiao-li Li[a], Jian-min Ma[a,b,*]

[a]*Key Laboratory for Environmental Pollution Prediction and Control, Gansu Province, College of Earth and Environmental Sciences, Lanzhou University, South Road of Tianshui, 222, Lanzhou 730000, China, email: linsy16@lzu.edu.cn (S. Lin), yyxu@lzu.edu.cn (Y. Xu), lixiaoli@lzu.edu.cn (X. Li), jmma@pku.edu.cn (J. Ma)*
[b]*Laboratory for Earth Surface Processes, College of Urban and Environmental Sciences, Peking University, Beijing 100000, China*

Received 8 October 2018; Accepted 27 March 2019

ABSTRACT

Polydopamine (PDA) functionalized NH_2-MIL-53(Al) nanoparticles (NH_2-MIL-53(Al)@PDA NPs) were successfully prepared by a facile *in-situ* polymerization method for the first time and characterized by various methods, including transmission electron microscopy (TEM), scanning electron microscopy (SEM), Fourier transform infrared (FT-IR) spectroscopy, X-ray diffraction (XRD) analysis, and Brunauer-Emmett-Teller (BET) analysis. The prepared NH_2-MIL-53(Al)@PDA NPs were used to remove cationic dyes crystal violet (CV) and malachite green (MG) from aqueous solutions. The maximum removal efficiency of NH_2-MIL-53(Al)@PDA NPs for CV and MG reached 95.94% and 77.88% at pH 10.0 and 8.0, respectively. Compared with NH_2-MIL-53(Al), NH_2-MIL-53(Al)@PDA NPs showed better adsorption capacity and removal efficiency. The adsorption of cationic dyes on NH_2-MIL-53(Al)@PDA NPs might be attributed to hydrogen bonding, electrostatic, and π-π interactions. The results indicate that pseudo-second-order models and Freundlich isotherm are a better fit for CV and MG adsorption. Adsorption thermodynamic tests showed that the adsorption was spontaneous, irreversible, and endothermic. NH_2-MIL-53(Al)@PDA NPs can be used for five times with no loss in absorption efficiency.

Keywords: Metal-organic frameworks; NH_2-MIL-53(Al)@PDA; Adsorption; Cationic dyes

1. Introduction

With extensive release of industrial effluents, organic dyes have been identified as harmful pollutants in the environment. Because of high toxicity, organic dyes pose a risk to aquatic ecosystem [1,2]. The colorful wastewater prevents the penetration of sunlight to rivers and lakes, thus reducing the photosynthesis of algae in water and affecting the activities of aquatic organisms [3]. Because of carcinogenic, teratogenic, and mutagenic characteristics, the dye pollutants also pose health risk to humans [4,5]. As common triphenylmethane type cationic synthetic dyes, crystal violet (CV) and malachite green (MG) (Fig. 1) are widely used in industries and medical products [6,7]. To reduce the exposure risk of organic dyes in environment and human population, removal of organic dyes from wastewater has become one of the top priorities.

Various techniques and methods have been used to remove organic dyes from aqueous solutions, such as adsorption, coagulation, flocculation, electrolysis, membrane separation, and biological oxidation [8–11]. In particular, the adsorption techniques have received much attention because of their low cost, simple operation, high efficiency, and environment-friendly characteristics [12]. Recently, different types of adsorbents such as clay minerals, carbon-based materials, magnetic materials, polymers, metal oxides, and metal-organic frameworks (MOFs) have been developed and used to remove organic dyes from contaminated water [13–16]. In particular, MOFs are a class of crystalline materials comprising of metal ions or metal clusters connected with organic ligands [17]. Compared with conventional porous materials, MOFs emerged as a novel

*Corresponding author.

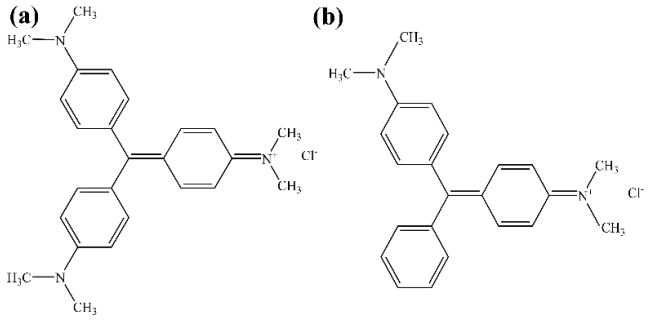

Fig. 1. Structures of CV (a) and MG (b).

class of nanoporous solids because of their easy tunability of pore size and shape, high thermal and mechanical stabilities, open metal sites in the skeleton, and high surface areas [18–20]. MOFs have been extensively applied in many field operations, such as gas storage and separation, catalysis, purification, sensors, drug delivery, and adsorption [21–26].

Among numerous MOFs, unlike zeolite-related inorganic hybrid materials, the synthesis of MIL series materials does not need an organic or inorganic template [27]. Rather, MIL can be combined with trivalent metal cations in the field of metal carboxylates and has special characteristics such as hydrothermal stability and a large surface area [28]. Because of these advantages, MIL has been widely used to remove dye pollutants in water. For example, g-C_3N_4/MIL-125(Ti) nanocomposites showed excellent photocatalytic performance for Rhodamine B degradation [29]. MIL-100(Fe) nanoparticles (NPs) were used for the adsorption of MG in aqueous solutions [30]. MIL-53(Cr) and MIL-101(Cr) were grafted with ethylenediamine for methyl orange (MO) adsorption [31]. MIL-53(Al) and mesostructured MIL-53(Al) showed a higher efficiency for the removal of bisphenol A (BPA) [32]. As a member of the MIL family, MIL-53(Al) has also attracted much attention because of its special property such as the breathing effect. In MIL-53(Al) NPs, the water molecules were connected to the skeleton by hydrogen bonding. When interacting with polar molecules, the channel is contracted or expanded owing to strong electrostatic interaction [33]. This has stimulated extensive studies, mainly focusing on the adsorption and separation properties of gas. Compared with MIL-53, NH_2-MIL-53(Al) can be used to modify –NH_2 groups as an organic ligand. NH_2-MIL-53(Al) forms hydrogen bonding with –OH groups on the skeleton and bridging oxygen atoms [34], enabling NH_2-MIL-53(Al) to better disperse and easily functionalized. Thus, modified NH_2-MIL-53(Al) has a good potential for applications in the reduction and removal of dye pollutants in aqueous solutions.

There is a growing interest in modifying MOFs with polymers because of the control of morphologies and designation of functional groups on the surface of MOFs NPs [35]. Studies have been also focused on polydopamine (PDA) because of its unique adhesion capability, forming a stable shell through an *in-situ* polymerization reaction without surface pretreatment. Abundant amino groups, hydroxyl groups, and benzene rings of PDA enhance its adsorption capacity for some pollutants in aqueous solutions [36]. Some other NPs coated with PDA have been used in the treatment of water pollutants. Dong et al. [37] designed a series of sub-nano thick polydopamine layer coated graphene oxide (PD/GO) and found that the synthetic material can selectively adsorb Eschenmoser structure dyes and heavy metal ions (Pb^{2+}, Cu^{2+}, Cd^{2+}, and Hg^{2+}). Moreover, Fe_3O_4@C NPs was synthesized by carbonizing Fe_3O_4@PDA and exhibited excellent performance for dye adsorption, as reported by Zhou et al. [38].

In this study, NH_2-MIL-53(Al)@PDA NPs were obtained by grafting PDA on the surface of NH_2-MIL-53(Al) through *in-situ* polymerization. The product was characterized by transmission electron microscopy (TEM), scanning electron microscopy (SEM), X-ray diffraction (XRD) analysis, Fourier transform infrared (FT-IR) spectroscopy, Brunauer-Emmett-Teller (BET) analysis, and zeta potential analysis. NH_2-MIL-53(Al)@PDA NPs were used to remove cationic dyes such as CV and MG. The influencing factors of adsorption, including reaction time, pH, and temperature, and adsorption properties such as adsorption kinetics, adsorption isotherms, adsorption thermodynamics, and ionic strength were measured. The adsorption mechanism and regeneration of NH_2-MIL-53(Al)@PDA NPs were also investigated.

2. Experimental methods

2.1 Materials

Aluminum nitrate nonahydrate ($Al(NO_3)_3{\cdot}9H_20$, ≥ 99.0%) was purchased from Kermel. 2-Aminoterephthalic acid (NH_2-H_2BDC, 99%) was obtained from Alfa Aesar. *N*,*N*-dimethylformamide (DMF, ≥99.5%) and sodium chloride (NaCl, ≥99.5%) were supplied by Rionlon. Tris(hydroxymethyl)aminomethane (Tris, Biochemical reagents, ≥99.0%) was obtained from Sinopharm Chemical Reagent Co., Ltd. Dopamine hydrochloride ($C_8H_{12}ClNO_2{\cdot}HCl$, 98%) was obtained from Macklin. CV was purchased from Tianjin Kaixin Chemical Industry Co., Ltd. MG was supplied by Shanghai Zhongqin Chemical Reagent Co., Ltd. Ethanol was obtained from Tianjin Yongda Chemical Reagent Co., Ltd. Hydrochloric acid (HCl) was purchased from Tianjin Damao Chemical Regent Factory. Sodium hydroxide (NaOH) was obtained from Tianjin Guangfu technology development Co., Ltd. Deionized water was used in all the experiments. All the mentioned chemicals were of analytical grade unless otherwise stated and used as received without further purification.

2.2. Preparation of NH_2-MIL-53(Al) and NH_2-MIL-53(Al)@PDA NPs

NH_2-MIL-53(Al) was synthesized following the hydrothermal method as previously reported [39]. First, $Al(NO_3)_3{\cdot}9H_2O$ (6.2 g) and NH_2-H_2BDC (3.0 g) were dissolved in deionized water (45.6 mL) by ultrasonic dispersion to form a homogeneous solution. Then, the mixture was transferred into a Teflon-lined stainless-steel autoclave and maintained at 423.15 K for 5 h, subsequently cooled to room temperature naturally. Finally, the obtained NH_2-MIL-53(Al) NPs were collected by centrifugation, washed with deionized water and ethanol several times, and dried at 343.15 K for 24 h. To further purify the prepared NH_2-MIL-53(Al) NPs, the sample was added to a Teflon-lined

stainless-steel autoclave containing DMF and treated at 423.15 K for 24 h.

NH_2-MIL-53(Al)@PDA NPs were synthesized by an *in-situ* polymerization method. 200 mg of NH_2-MIL-53(Al) was dissolved in 100 mL of 0.1 M of Tris-HCl solution at pH 8.5. Then, 200 mg dopamine hydrochloride was added to the above mixture, and the mixture was stirred at room temperature for 24 h. The prepared NH_2-MIL-53(Al)@PDA NPs were washed with deionized water and ethanol and finally dried at 343.15 K for 24 h for further use.

2.3. Characterization

The morphology, shape, and size of the prepared NPs were measured using TEM (TECNAI G^2, FEI, USA) and SEM (JSM-6701F, Jeol, Japan). The crystal structures of the synthesized materials were determined using XRD (X' Pert PRO, PANalytical B.V., NLD). FT-IR spectra of the prepared NPs were obtained using a FT-IR spectrometer (NEXUS 670, Nicolet, USA). Surface areas of the samples were determined by BET analysis (TriStar II 3020, Micromeritics, USA). The charge of material was measured using a zeta potential instrument (Zetasizernano 3600, Malvern Instruments Ltd., UK). The concentrations of solution were measured using a UV-Vis spectrophotometer (EVO300 PC, Thermo Fisher Scientific, USA). Adsorption was carried out in a thermostatic oscillator (THZ-100, Shanghai YiHeng Scientific Instruments Co., Ltd, China).

2.4. Adsorption experiments

The stock solutions of CV and MG (1.0 g·L^{-1}) were prepared by dissolving CV and MG in deionized water and diluted to appropriate concentrations. Adsorption was carried out as follows: 5 mg of NH_2-MIL-53(Al)@PDA NPs was dispersed in 10 mL of CV or MG solutions at different concentrations from 10 to 60 mg·L^{-1}. Then, the solution was shaken in thermostatic oscillators at 250 rpm and constant temperatures of 288.15, 298.15, and 308.15 K. To evaluate the effect of pH on the removal of CV and MG from aqueous solutions, the pH of the solution was maintained from 4.0 to 10.0 using certain amounts of dilute HCl and NaOH solutions. After the adsorption, the solution was obtained by filtrating through a syringe filter (Sangchen, hydrophobic, 0.22 μm) and measured using a UV-Vis spectrophotometer at 578 and 612 nm for CV and MG, respectively. Each experiment was conducted with three parallel samples. The adsorbents were recycled by washing thoroughly with ethanol. The flow chart of experimental procedure is shown in Fig. 2.

The adsorption performances of NH_2-MIL-53(Al)@PDA NPs for CV and MG were studied from adsorption quantity (q_e) and removal efficiency, which can be calculated using the following equations:

$$q_e = \frac{(C_o - C_e)V}{m} \tag{1}$$

$$Removal(\%) = \frac{(Co - C_e)}{C_o} \times 100\% \tag{2}$$

where q_e (mg·g^{-1}) is the quantity of dye adsorbed on the adsorbents; C_0 and C_e (mg·L^{-1}) are the initial and final concentrations of CV and MG solutions, respectively. V (L) and m (g) in Eq. (1) are the volume and mass of adsorbents in CV and MG solutions, respectively.

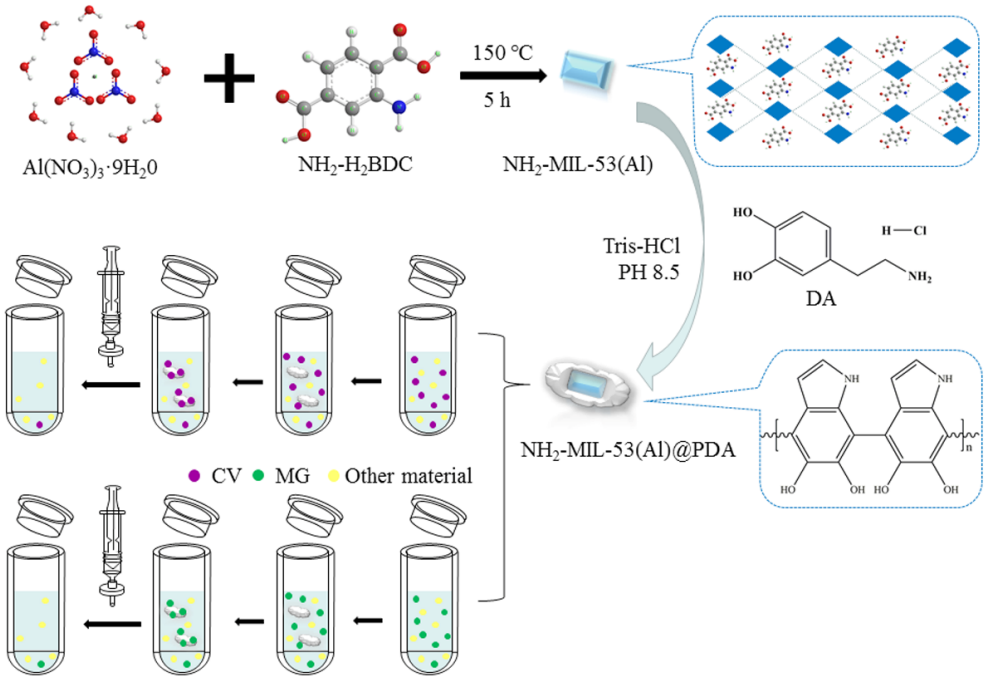

Fig. 2. Synthesis and adsorption of NH_2-MIL-53(Al)@PDA NP.

3. Results and discussion

3.1. Characterization of adsorbents

The XRD spectral analysis shows the crystal structure of NH_2-MIL-53(Al) and NH_2-MIL-53(Al)@PDA NPs. The XRD patterns of NH_2-MIL-53(Al) and NH_2-MIL-53(Al)@PDA NPs are shown in Fig. 3. As shown in Fig. 3a, all the diffraction peaks were consistent with the standard data of crystalline NH_2-MIL-53(Al) as reported previously [40,41]. This indicates that the crystals of NH_2-MIL-53(Al) were synthesized successfully. The strengthening peak signals of NH_2-MIL-53(Al) might be induced by the residual water molecules in the pore with a weak coordination with skeleton [41]. For NH_2-MIL-53(Al)@PDA NPs (Fig. 3b), the typical diffraction angles were 9.24°, 12.33°, 17.65°, 24.85°, and 27.03° corresponding with NH_2-MIL-53(Al) nanomaterials. This indicates that NH_2-MIL-53(Al)@PDA NPs still had a crystal structure after modifying with PDA.

The FT-IR spectra were used to identify the functional groups of NH_2-MIL-53(Al) and NH_2-MIL-53(Al)@PDA NPs. For NH_2-MIL-53(Al) (Fig. 4a), the strong adsorption peak at 777.4 cm^{-1} was assigned to the -CH stretching vibration of benzene ring. The absorption bands at 1256.7 cm^{-1} and 1336.5 cm^{-1} were attributed to -C-N(NH_2) stretching vibrations [41]. The peak centered on 1441.9 cm^{-1} was assigned to the symmetrical stretching vibration of carbonyl group. The peak appearing at 1494.9 cm^{-1} can be assigned to the dissymmetrical stretching vibration of carbonyl group coordinated with Al^{3+}. The adsorption peak at 1671.2 cm^{-1} might be the result of carbonyl group of DMF molecules adhered to the channels [42]. After coating with PDA as shown in Fig. 4b, the absorption bands at 3388.0 cm^{-1} and 3493.4 cm^{-1} were attributed to the vibrations of NH_2 on NH_2-MIL-53(Al)@PDA NPs. The peak at 3424.0 cm^{-1} corresponded to the hydrogen bonding stretching vibration of OH on PDA [43]. These results indicate that PDA was successfully modified on NH_2-MIL-53(Al) nanomaterials.

TEM and SEM were used to characterize the morphology of synthesized NH_2-MIL-53(Al) and NH_2-MIL-53(Al)@PDA NPs. As shown in Figs. 5a and 5c, the rhomboid shaped morphological structure of as-prepared NH_2-MIL-53(Al) samples was consistent with others reported in the literature [43]. The TEM and SEM images of NH_2-MIL-53(Al)@PDA NPs are shown in Figs. 5b and 5d. Compared with NH_2-MIL-53(Al), the form of NH_2-MIL-53(Al)@PDA NPs became round and had a thin shell on their surface, indicating that PDA was successfully modified on the surface of NH_2-MIL-53(Al). The crystal sizes of NH_2-MIL-53(Al) and NH_2-MIL-53(Al)@PDA NPs were 50–300 nm and 80–360 nm, respectively. The BET surface area of NH_2-MIL-53(Al) and NH_2-MIL-53(Al)@PDA NPs were 182.3051 $m^2 \cdot g^{-1}$ and 83.7430 $m^2 \cdot g^{-1}$, respectively.

3.2. Effect of pH

The initial pH of CV and MG solutions is an important parameter, controlling the adsorption, particularly the removal efficiency. Fig. 6a shows the effect of solution pH on the adsorption of CV and MG with NH_2-MIL-53(Al)@PDA NPs at 298.15 K. As shown in Fig. 6a, the adsorption quantity and removal efficiency first increased with the increase in pH from 4.0 to 8.0 for MG and then decreased from 8.0 to 9.0. At pH 8.0, the maximum adsorption quantity and removal efficiency for MG were 51.11 $mg \cdot g^{-1}$ and 85.66%, respectively. However, for CV, the adsorption capacity increased in the pH range from 4.0 to 10.0. Thus, pH 10.0 was selected as the best condition for the adsorption of CV. The maximum adsorption quantity and removal efficiency for CV were 55.72 $mg \cdot g^{-1}$ and 92.86%, respectively. As members of common cationic synthetic dyes, CV and MG might have a strong electrostatic attraction with the hydroxyl groups on the surface of NH_2-MIL-53(Al)@PDA NPs. This pH range was mainly selected because of the dye reagent which might be converted to other compounds, and because the structure of NH_2-MIL-53(Al)@PDA NPs may collapse when pH is above 9.0 and 10.0 for CV and MG, respectively.

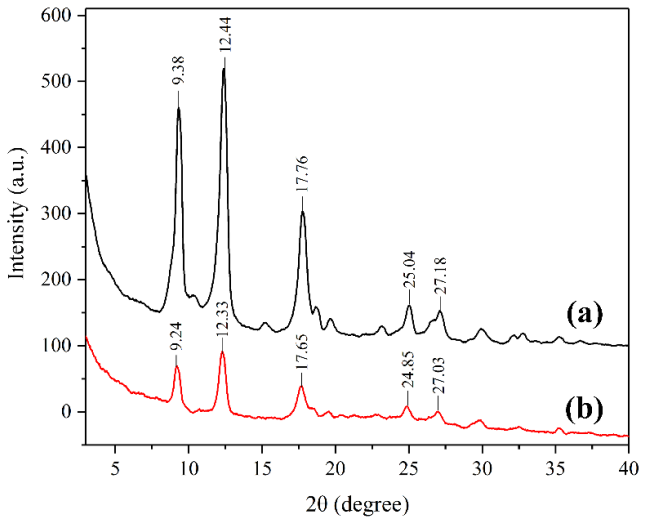

Fig. 3. XRD patterns of NH_2-MIL-53(Al) (a) and NH_2-MIL-53(Al)@PDA NPs (b).

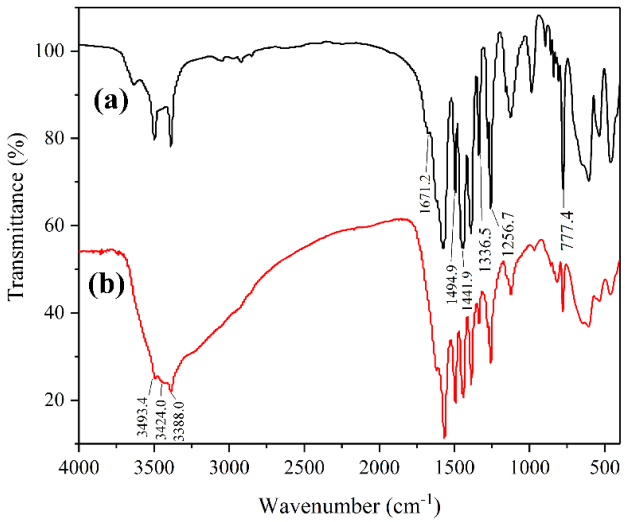

Fig. 4. FT-IR spectra of NH_2-MIL-53(Al) (a) and NH_2-MIL-53(Al)@PDA NPs (b).

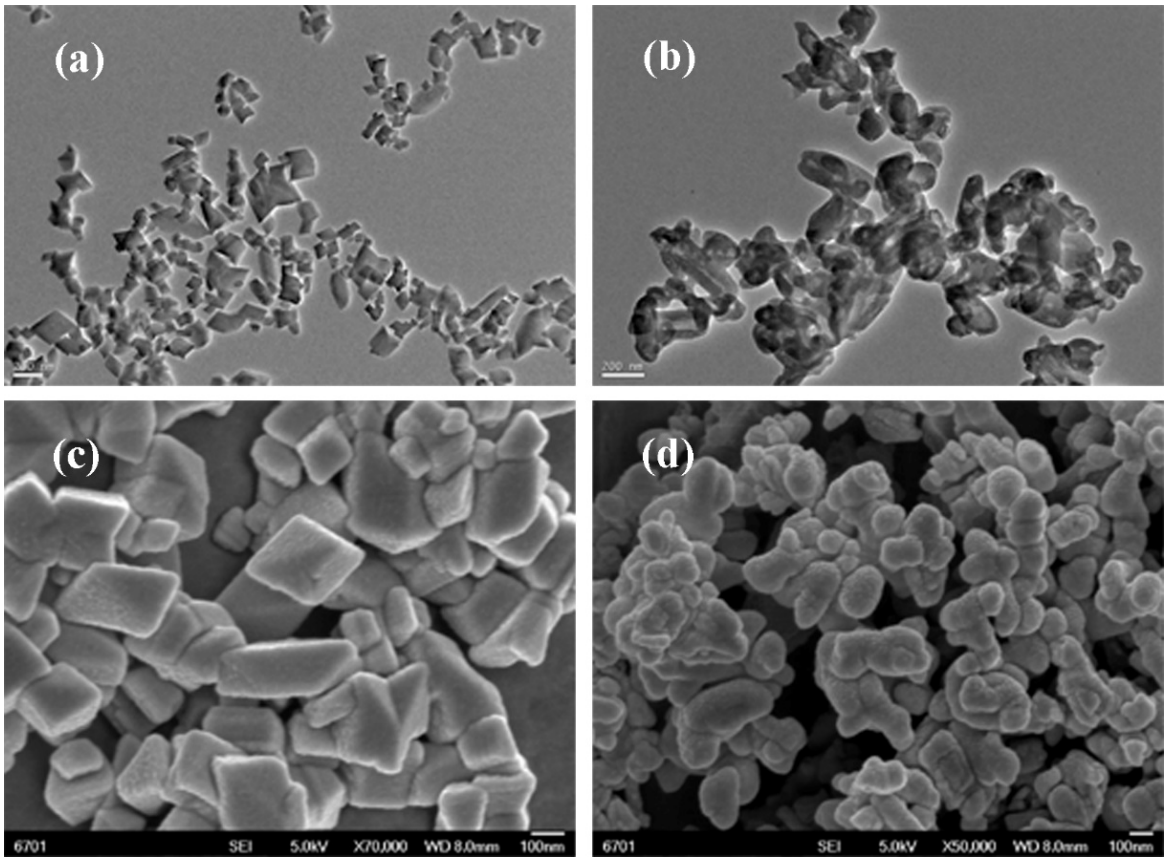

Fig. 5. TEM images of NH_2-MIL-53(Al) (a) and NH_2-MIL-53(Al)@PDA NPs (b). SEM images of NH_2-MIL-53(Al) (c) and NH_2-MIL-53(Al)@PDA NPs (d).

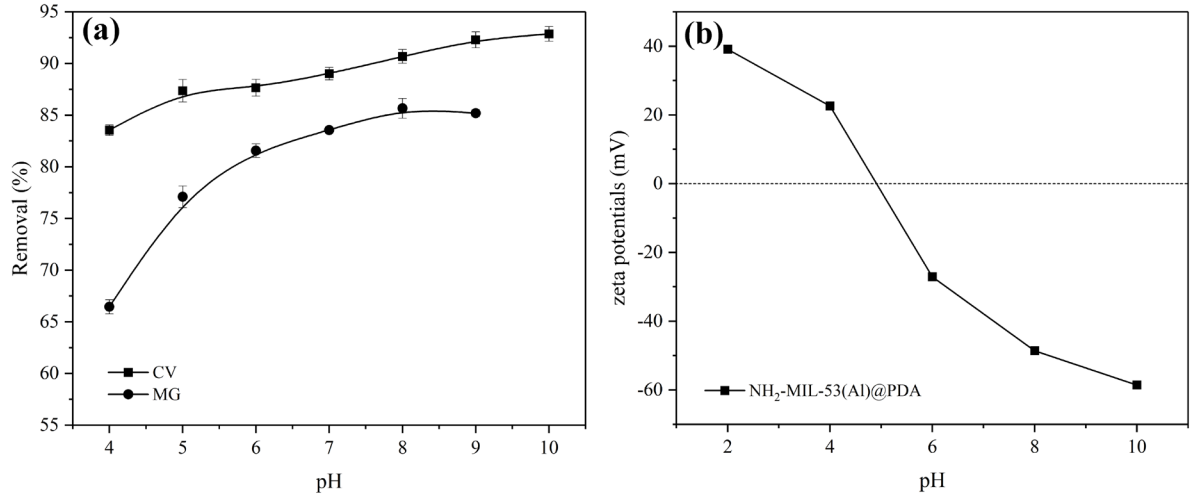

Fig. 6. Effect of solution pH on the adsorption of CV and MG on NH_2-MIL-53(Al)@PDA NPs (a). Effect of pH on the zeta potential of NH_2-MIL-53(Al)@PDA NPs (b). (*m*: 5 mg; C_0: 30 mg·L^{-1}; *V*: 10 mL; *T*: 298.15 K; *t*: 100 min; pH: 4 - 10 and 4 - 9 for CV and MG, respectively.)

The tendency of MG and CV adsorption can be explained by the zeta potential of NH_2-MIL-53(Al)@PDA NPs. Zeta potential reflects the charge on the surface of adsorbent at different pH. At pH_{PZC} (point of zero charge), the surface charge is zero, often used to quantify the charge characteristics of an adsorbent surface [44]. When pH > pH_{PZC}, the surface charge is negative. The surface charge becomes positive when pH < pH_{PZC} [45]. As shown in Fig. 6b, the surface charge of NH_2-MIL-53(Al)@PDA NPs changed from positive to negative with pH ranging from 2.0 to 10.0. The pH_{PZC} was obtained

with pH 5.0–6.0. As reported, the pKa values of CV and MG were 9.4 and 6.9 at 298.15 K, respectively [46]. For CV, the surface charge of CV molecule was positive with pH of 4.0–9.0. Therefore, the removal efficiency increased, mainly because of the constantly strengthened electrostatic interaction between CV and NH_2-MIL-53(Al)@PDA NPs. At pH 10.0, both the molecular surfaces of NH_2-MIL-53(Al)@PDA and CV were full of negative charges. This should exhibit strong electrostatic repulsion, but the removal efficiency reaches the maximum. This indicates the existence of other reaction mechanisms besides electrostatic reaction. For MG, the charge of MG surface was positive with pH of 4.0–6.9. As a result, the removal efficiency gradually increased, mainly due to the electrostatic interaction. Both MG and NH_2-MIL-53(Al)@PDA NPs surface had a negative charge with pH > 6.9. This indicates that some other processes could control the adsorption, such as hydrogen bonding interaction and π-π interactions.

3.3. Effect of contact time and adsorption kinetics

Fig. 7 shows the effect of contact time on the adsorption of CV and MG with NH_2-MIL-53(Al)@PDA NPs at 298.15 K. As shown in Fig. 7, the removal efficiency of CV and MG rapidly increased within 100 min. The optimal removal efficiencies of 90.67% for CV and 67.68% for MG were achieved at 100 min. Subsequently, the removal efficiency had no obvious change with the increase in contact time from 100 min to 600 min. In the beginning, rapid adsorption occurs because of large quantities of active sites on the surface of NH_2-MIL-53(Al)@PDA NPs. With the increase in adsorption time, more and more active sites are gradually occupied by dye pollutants, leading to slower adsorption of CV and MG.

The adsorption kinetics can help to explore whether the adsorption mechanism is chemical adsorption and polyphase catalysis. Pseudo-first-order and pseudo-second-order kinetic models were applied to elucidate the adsorption mechanism. The equations of these two kinetic models are as follows [47,48].

$$\ln\left(q_e - q_t\right) = \ln q_e - k_1 t \tag{3}$$

$$\frac{t}{q_t} = \frac{1}{k_2 {q_e}^2} + \frac{t}{q_e} \tag{4}$$

$$h = k_2 q_e^2 \tag{5}$$

where q_e and q_t (mg·g^{-1}) are the adsorption quantities at equilibrium time and time t, respectively; k_1 (min^{-1}) is the pseudo-first-order equilibrium rate constant; k_2 (g·mg^{-1}·min^{-1}) is the pseudo-second-order rate constant; h (mg·g^{-1}·min^{-1}) is the initial adsorption rate. The value of k_1 in Eq. (3) was calculated from the plots of ln(q_e–q_t) vs. time. The fittings of pseudo-first-order and pseudo-second-order models are shown in Figs. 7a and 7b, respectively.

Compared with the correlation coefficients (R^2) shown in Table 1, the R^2 values of CV and MG adsorption in the pseudo-second-order model were 0.9998 and 0.9991, respectively, much higher than the pseudo-first-order model. The $q_{e,exp}$ values of pseudo-second-order model for CV and MG adsorption were 57.67 and 47.65 mg·g^{-1}, respectively. These two values are close to the experimental values of 57.57 and 46.74 mg·g^{-1} for CV and MG, respectively. Therefore, the adsorption of CV and MG follows the pseudo-second-order kinetic model. It is assumed that the adsorption mechanism and rate limiting step are mainly chemisorption. Because of the presence of amino and catechol groups on the surface of NH_2-MIL-53(Al)@PDA NPs, hydrogen bonding or electron exchange is possible with the dimethylamino and other groups on dye pollutions.

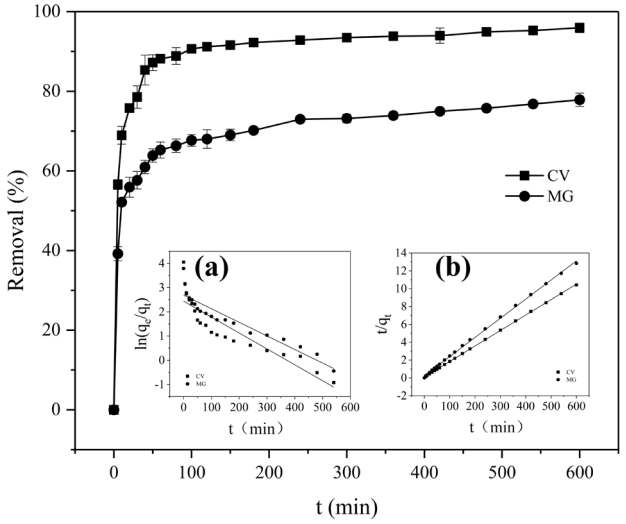

Fig. 7. Effect of contact time on the adsorption of CV and MG on NH_2-MIL-53(Al)@PDA NPs. Insets show (a) the pseudo-first-order, and (b) pseudo-second-order kinetic models. (m: 50 mg; C_0: 30 mg·L^{-1}; V: 100 mL; T: 298.15 K; t: 0–600 min for CV and MG, respectively.)

3.4. Adsorption isotherms

Adsorption isotherms reflect the adsorption capacity that varies with the equilibrium concentration at a certain temperature. As shown in Fig. 8, the adsorption quantity of CV (a) and MG (b) increased with the initial concentration increasing at the same temperature. The adsorption quantity of CV and MG also increased with the temperature increasing at the same initial concentration. Langmuir, Freundlich, and Temkin isotherms were used to evaluate the properties of adsorbent surface and adsorption behaviors. The equations of the three isotherms are as follows [48–50].

$$\frac{C_e}{q_e} = \frac{1}{q_m K_L} + \frac{C_e}{q_m} \tag{6}$$

$$\ln q_e = \ln K_F + \left(\frac{1}{n}\right)\ln C_e \tag{7}$$

$$q_e = B\ lnK_T + B\ln C_e \tag{8}$$

where q_e (mg·g^{-1}) is the adsorption quantity at the equilibrium time, taken as 100 min in this study; q_m (mg·g^{-1}) is the Langmuir constant indicating the maximum adsorption capacity; C_e (mg·L^{-1}) is the concentration of dye solution at the equilibrium time. K_L (L·mg^{-1}) is the Langmuir constant,

Table 1
Pseudo-first-order and pseudo-second-order model constants for the adsorption of CV and MG on NH_2-MIL-53(Al)@PDA NPs

Dyes	Pseudo-first order model				Pseudo-second order model			
	$q_{e,exp}$ (mg·g^{-1})	$q_{e,cal}$ (mg·g^{-1})	k_1 (min^{-1})	R^2	$q_{e,cal}$ (mg·g^{-1})	h (mg·g^{-1}·min^{-1})	k_2 (g·mg^{-1}·min^{-1})	R^2
CV	57.57	11.48	6.6×10^{-3}	0.7904	57.67	9.350	2.8×10^{-3}	0.9998
MG	46.73	14.90	5.6×10^{-3}	0.8732	46.75	3.682	1.7×10^{-3}	0.9991

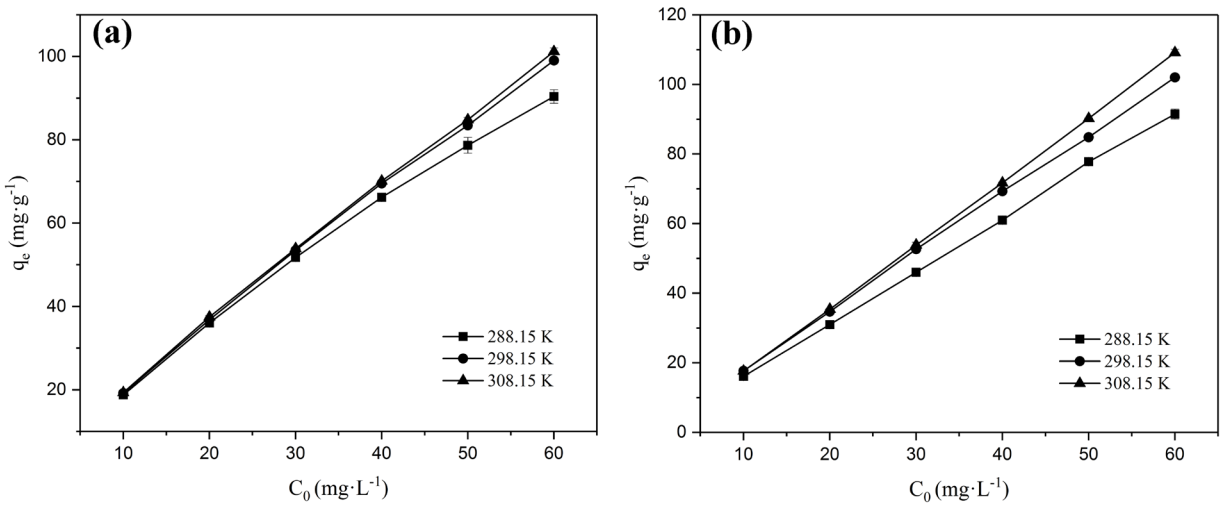

Fig. 8. Adsorption isotherms of CV (a)and MG (b) on NH_2-MIL-53(Al)@PDA NPs at 288.15 K, 298.15 K, and 308.15 K. (m: 5 mg; C_0: 10–60 mg·L^{-1}; V: 10 mL; T: 288.15, 298.15, and 308.15 K; t: 100 min for CV and MG, respectively.)

an adsorption equilibrium constant including the affinity of binding sites. K_F (mg·g^{-1}) in Eq. (7) is the Freundlich constant related to adsorption capacity. Parameter n (g·L^{-1}) represents the strength of driving force of adsorption. K_T (mol^{-1}) in Eq. (8) is the equilibrium binding constant corresponding to the maximum binding energy; B is the heat of adsorption. K_F and n can be calculated from the intercept and slope of the linearized plot of ln q_e vs. ln C_e, respectively.

The adsorption constants and correlation coefficients (R^2) of Langmuir, Freundlich, and Temkin at different temperatures are shown in Table 2. For CV, the R^2 values of Freundlich isotherm were 0.9988, 0.9995, and 0.9975 at 288.15, 298.15, and 308.15 K, respectively. The R^2 values of Freundlich isotherm for MG adsorption were 0.9981, 0.9981, and 0.9974 at 288.15, 298.15, and 308.15 K, respectively. These values were much higher than other isotherms, indicating that the adsorption of CV and MG on NH_2-MIL-53(Al)@PDA NPs can be better described by Freundlich isotherm.

Freundlich isotherm is based on an empirical equation assuming that the adsorption system can be monolayer and multilayer. Moreover, the adsorption occurs on a heterogeneous surface [36]. Therefore, both chemical and physical adsorption should be considered for CV and MG adsorption. Considering different temperatures, the values of $1/n$ in CV and MG adsorption were all less than 1 and decreased with the temperature increasing. This phenomenon indicated that the adsorption was more favorable with the temperature increasing [48]. The results illustrated that the adsorption was endothermic.

3.5. Adsorption thermodynamics

To understand the extent and driving force of adsorption process on NH_2-MIL-53(Al)@PDA, adsorption free energy (ΔG^o), standard enthalpy (ΔH^o), and standard entropy (ΔS^o) were used to calculate the adsorption of CV and MG at 288.15, 298.15, and 308.15 K. The adsorption was achieved by adding 5 mg of NH_2-MIL-53(Al)@PDA NPs to 10 mL of CV or MG solution with a concentration of 30 mg·L^{-1}.

The relationships between ΔG^o, ΔH^o, and ΔS^o can be defined as follows [44,51].

$$\ln b = \frac{\Delta S^\circ}{R} - \frac{\Delta H^\circ}{RT} \tag{9}$$

$$\ln b = 2.303 \log\left(\frac{q_e}{C_e}\right) \tag{10}$$

$$\Delta G^\circ = \Delta H^\circ - T\Delta S^\circ \tag{11}$$

where q_e (mg·g^{-1}) is the adsorption quantity at the equilibrium time. C_e (mg·L^{-1}) is the concentration of the dye solution at equilibrium time; T (K) is the absolute temperature of solution; R is the ideal gas constant (8.314 J·mol^{-1}·K^{-1}); b is the equilibrium binding constant (L·mg^{-1}). The values of ΔH^o and ΔS^o can be obtained from the slope and intercept of linear regression relationship between ln b and 1/T.

Table 2
Langmuir, Freundlich, and Temkin adsorption constants of CV and MG on NH_2-MIL-53(Al)@PDA NPs

Dyes	Temp (K)	Langmuir parameter			Freundlich parameter			Temkin parameter		
		q_m (mg·g^{-1})	K_L (L·mg^{-1})	R^2	K_F (mg·g^{-1})	n (g·L^{-1})	R^2	B	K_T (mol^{-1})	R^2
CV	288.15	106.6	0.261	0.9495	18.81	1.911	0.9988	21.58	3.165	0.9349
	298.15	126.6	0.278	0.9453	29.54	1.943	0.9995	24.51	3.794	0.9236
	308.15	122.1	0.336	0.9318	32.44	2.079	0.9975	23.01	5.021	0.9064
MG	288.15	622.3	0.011	0.7078	7.750	1.071	0.9981	39.43	0.578	0.9249
	298.15	299.1	0.055	0.8898	16.70	1.217	0.9981	38.85	1.161	0.9219
	308.15	116.4	0.142	0.9237	18.834	1.868	0.9974	22.92	1.845	0.9126

The values of thermodynamic constants for the adsorption of CV and MG on NH_2-MIL-53(Al)@PDA NPs are shown in Table 3. According to [52], when ΔG^o is negative, the adsorption can be spontaneous. The value of ΔG^o between –80 and –400 kJ·mol^{-1} or –20 and 0 kJ·mol^{-1} indicates that the adsorption can be either chemical or physical adsorption. As shown in Table 4, the value of ΔG^o ranges from –6.750 to –8.497 kJ·mol^{-1} and from –5.243 to –7.939 kJ·mol^{-1} for CV and MG, respectively, indicating that the adsorption was spontaneous and irreversible. The absolute values of ΔG^o gradually increased with the increase in temperature, indicating that a higher temperature strengthens the spontaneous adsorption process. The result shows that physical adsorption is the main driving force in the first adsorption process. As shown in Table 3, the ΔH^o values for CV and MG adsorption are 18.42 and 33.60 kJ·mol^{-1}, respectively. These positive values verify that the adsorption of CV and MG on NH_2-MIL-53(Al)@PDA NPs is an endothermic process. The result is consistent with the fact that the removal efficiency gradually increased with increasing temperature. The values of ΔS^o are 87.35and 134.8J·mol^{-1}·K^{-1} for CV and MG adsorption, respectively, suggesting that the adsorption is associated with entropy increase.

Table 3
Thermodynamic constants for the adsorption of CV and MG on NH_2-MIL-53(Al)@PDA NPs

Dyes	ΔH^o (kJ·mol^{-1})	ΔS^o (J·mol^{-1}·K^{-1})	ΔG^o(kJ·mol^{-1})		
			288.15 (K)	298.15 (K)	308.15 (K)
CV	18.42	87.35	–6.750	–7.623	–8.497
MG	33.60	134.8	–5.243	–6.591	–7.939

3.6. Ionic strength

An increase in ionic strength of solution affects the removal efficiency of NH_2-MIL-53(Al)@PDA NPs. Fig. 9 shows the effect of ionic strength on the adsorption of CV and MG on NH_2-MIL-53(Al)@PDA NPs by a NaCl solution. As shown in Fig. 9, the removal rates reached the maximum value at 89.02% and 72.55% for CV and MG adsorption without NaCl in the solution, respectively. Then, the adsorption efficiency for CV and MG gradually decreased with the increase in NaCl concentration from 0.0 to 0.2 mol L^{-1}. Compared with CV, the removal efficiency of MG decreased significantly. This can be attributed to the thinning of electrical double layer with increasing concentration of NaCl. Except that, the equilibrium charge ions surrounding the available active sites with opposite charges resulted in a charge neutralization. Therefore, the electrostatic interaction between dye pollutants and NH_2-MIL-53(Al)@PDA NPs weakened with increasing concentration of NaCl.

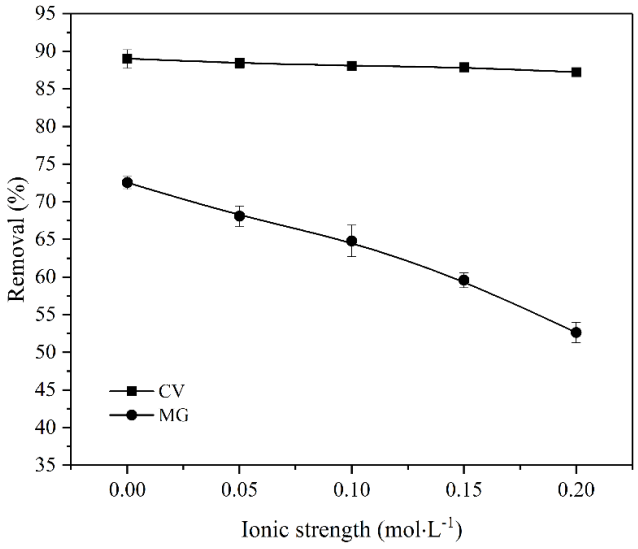

Fig. 9. Effect of ionic strength on the adsorption of CV and MG on NH_2-MIL-53(Al)@PDA NPs. (m: 5 mg; C_0: 30 mg·L^{-1}; V: 10 mL; T: 298.15 K; t: 100 min; NaCl concentration: 0.0–0.2 mol·L^{-1} for CV and MG, respectively.)

3.7. Regenerability of NH_2-MIL-53(Al)@PDA NPs

Reusability reflects the stability of NH_2-MIL-53(Al)@PDA NPs. The results of five consecutive adsorption-desorption cycles are shown in Fig. 10. Ethanol was selected as the desorption solvent to evaluate the regeneration and reusability of NH_2-MIL-53(Al)@PDA. Initially, the removal efficiencies of CV and MG solution were 83.66% and 80.02%, respectively. As shown in Fig. 10, the removal efficiency did not significantly change in the following three cycles because of its stable structure.

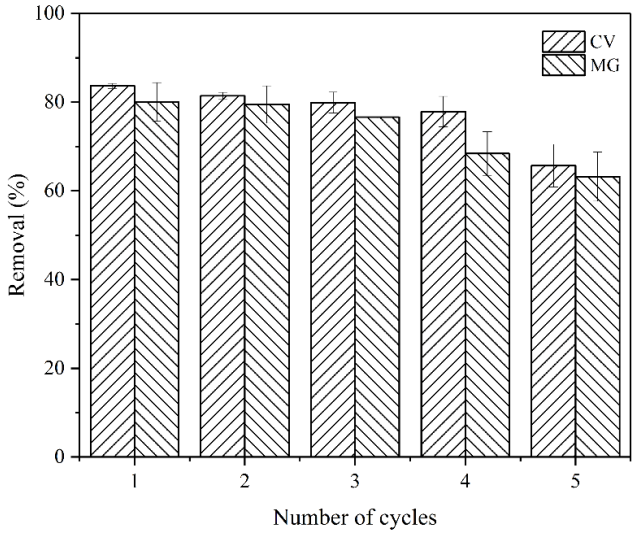

Fig. 10. Reusability of NH_2-MIL-53(Al)@PDA NPs for the adsorption of CV and MG. (*m*: 20 mg; C_0: 30 mg·L^{-1}; *V*: 40 mL; *T*: 298.15 K; *t*: 100 min for CV and MG, respectively.)

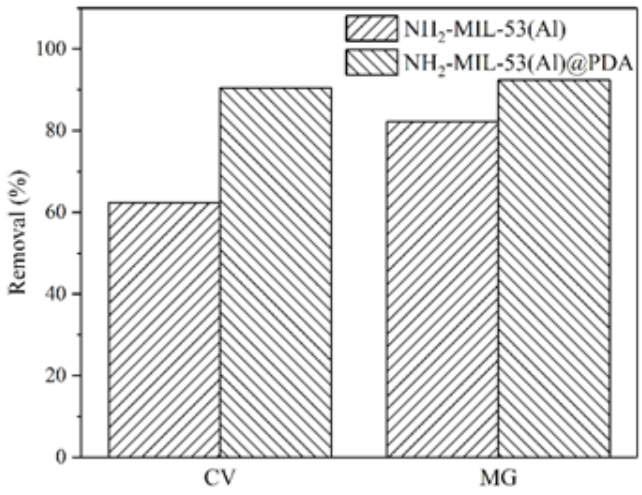

Fig. 11. Comparison of adsorption effect for CV and MG with NH_2-MIL-53(Al) and NH_2-MIL-53(Al)@PDA NPs. (*m*: 5 mg; C_0: 30 mg·L^{-1}; *V*: 10 mL; *T*: 308.15 K; *t*: 100 min; pH 10.0 and pH 8.0 for CV and MG, respectively.)

3.8. Comparison of adsorption effect between NH_2-MIL-53(Al) and NH_2-MIL-53(Al)@PDA NPs

The removal rates of CV and MG on NH_2-MIL-53(Al) and NH_2-MIL-53(Al)@PDA NPs under the optimal conditions are shown in Fig. 11. As shown in Fig. 11, the adsorption efficiency of NH_2-MIL-53(Al)@PDA NPs significantly increased compared with NH_2-MIL-53(Al). For CV and MG, the removal efficiencies were 62.34% and 82.24% on NH_2-MIL-53(Al). However, the removal efficiency increased to 90.51% and 92.37% with NH_2-MIL-53(Al)@PDA NPs. This result shows that the modification of PDA on NH_2-MIL-53(Al) improved the removal efficiency of dye pollutants.

3.9. Adsorption mechanism

As mentioned above, the adsorption is associated with multiple reaction mechanisms. First, NH_2-MIL-53(Al) had a breathing effect as reported;this might affect the removal efficiency [33], can be attributed to the two structures of NH_2-MIL-53(Al), namely, narrow-pore and large-pore structures. The former has a smaller cell and pore volume; the latter has larger and more open pores. When adsorbing CV and MG, the narrow-pore structure is switched to the large-pore structure by changing the shape of original structure to increase coverage. Second, the zeta potential of NH_2-MIL-53(Al)@PDA, showed that the surface of adsorbent was negative at pH 6.0–10.0, promoting the electrostatic interaction between NH_2-MIL-53(Al)@PDA NPs and cationic dye pollutants. Third, aggregation of PDA enables the surface of NH_2-MIL-53(Al)@PDA NPs to contain many hydroxyl groups, thus increasing the binding sites with dye pollutions [53]. Moreover, NH_2-MIL-53(Al)@PDA NPs are combined with dimethylamino groups through hydrogen bonding. Fourth, the structures of both CV and MG contain aromatic rings. NH_2-MIL-53(Al)@PDA NPs also contain abundant aromatic backbone, inducing π-π interactions between dye molecules and adsorbent [54]. Finally, as shown in Fig. 11, under the optimal conditions, the removal efficiency of MG was better than CV with NH_2-MIL-53(Al)@PDA NPs as the adsorbing material. This can be attributed to the different steric effects of CV and MG. The molecular size of CV (13.90–14.32 Å) is larger than MG (11.57–14.32 Å), as calculated by ChemDraw. Therefore, MG could be captured easily by NH_2-MIL-53(Al)@PDA NPs.

4. Conclusions

In summary, NH_2-MIL-53(Al)@PDA NPs were successfully synthesized following an *in-situ* polymerization method. The prepared NH_2-MIL-53(Al)@PDA NPs with a high removal efficiency were used to successfully adsorb CV and MG from aqueous solutions. Under the optimal adsorption conditions, the removal efficiency reached 90.51% and 92.37% for CV and MG, respectively. The adsorption kinetics and isotherms were determined as the pseudo-second-order kinetic model and Freundlich isotherm, respectively. The calculated Gibbs free energy showed that the adsorption was spontaneous and irreversible. The estimated entropy change showed that the adsorption was endothermic. Electrostatic, hydrogen bonding, and π-π interactions were the main interactions occurring between NH_2-MIL-53(Al)@PDA NPs and dye pollutants. The removal efficiency did not change significantly after reuse for five times.

Acknowledgments

The authors are grateful for financial support from the National Natural Science Foundation of China (Grant Nos. 41603087) and Fundamental Research Funds for the Central University (nos. lzujbky-2018-145 and lzujbky-2017-218).

Compliance with ethical standards

Conflict of interest

List of symbols

b — The equilibrium binding constant
t — Reaction time
q_e — The adsorption quantity at equilibrium time
q_t — The adsorption quantity at time t
q_m — The Langmuir constant demonstrating maximum adsorption capacity
C_0 — Initial concentration
C_e — Final concentration
V — The volume of solution
m — The mass of adsorbent
k_1 — The pseudo-first-order equilibrium rate constant
k_2 — The pseudo-second-order rate constant
K_L — The Langmuir constant
K_F — The Freundlich constant
K_T — The equilibrium binding constant
h — The initial adsorption rate
B — The heat of adsorption

References

[1] J. Hu, W. Dai, X.Y. Yan, Comparison study on the adsorption performance of methylene blue and congo red on Cu-BTC, Desal. Water Treat., 57 (2016) 4081–4089.
[2] M.R. Azhar, H.R. Abid, M.O. Tade, V. Periasamy, H.Q. Sun, S.B. Wang, Cascade applications of robust MIL-96 metal organic frameworks in environmental remediation: Proof of concept, Chem. Eng. J., 341 (2018) 262–271.
[3] E. Haque, J.W. Jun, S.H. Jhung, Adsorptive removal of methyl orange and methylene blue from aqueous solution with a metal-organic framework material, iron terephthalate (MOF-235), J. Hazard. Mater., 185 (2011) 507–511.
[4] H. Demir, A. Top, D. Balköse, S. Ülkü, Dye adsorption behavior of Luffa cylindrica fiber, J. Hazard. Mater., 153 (2008) 389–394.
[5] L.H. Ai, C.Y. Zhang, F. Liao, Y. Wang, M. Li, L.Y. Meng, J. Jiang, Removal of methylene blue from aqueous solution with magnetite loaded multi-wall carbon nanotube: Kinetic, isotherm and mechanism analysis, J. Hazard. Mater., 198 (2011) 282–290.
[6] S. Loera-serna, E. Ortiz, H.I. Beltrán, First trial and physicochemical studies on the loading of basic fuchsin, crystal violet and Black Eriochrome T on HKUST-1, New J. Chem., 41 (2017) 3097–3105.
[7] A. Mittal, V. Gajbe, J. Mittal, Removal and recovery of hazardous triphenylmethane dye, Methyl Violet through adsorption over granulated waste materials, J. Hazard. Mater., 150 (2008) 364–375.
[8] X.P. Luo, S.Y. Fu, Y.M. Du, J.Z. Guo, B. Li, Adsorption of methylene blue and malachite green from aqueous solution by sulfonic acid group modified MIL-101, Micropor. Mesopor. Mater., 237 (2017) 268–274.
[9] A.K. Verma, R.R. Dash, P. Bhunia, A review on chemical coagulation/flocculation technologies for removal of colour from textile wastewaters, J. Environ. Manage., 93 (2012) 154–168.
[10] I. Sirés, E. Brillas, M.A. Oturan, M.A. Rodrigo, M. Panizza, Electrochemical advanced oxidation processes: today and tomorrow. A review, Environ. Sci. Pollut. Res., 21 (2014) 8336–8367.
[11] E. Forgacs, T. Cserháti, G. Oros, Removal of synthetic dyes from wastewaters: a review, Environ. Int., 30 (2004) 953–971.
[12] M.R. Azhar, H.R. Abid, H.Q. Sun, V. Periasamy, M.O. Tadé, S.B. Wang, Excellent performance of copper based metal organic framework in adsorptive removal of toxic sulfonamide antibiotics from wastewater, J. Colloid Interface Sci., 478 (2016) 344–352.
[13] V. Vimonses, S.M. Lei, B. Jin, C.W.K. Chow, C. Saint, Kinetic study and equilibrium isotherm analysis of Congo Red adsorption by clay materials, Chem. Eng. J., 148 (2009) 354–364.
[14] W.T. Wang, S. Chakrabarti, Z.G. Chen, Z.F. Yan, M.O. Tade, J. Zou, Q. Li, A novel bottom-up solvothermal synthesis of carbon nanosheets, J. Mater. Chem. A, 2 (2014) 2390–2396.
[15] X.W. Liu, T.J. Sun, J.L. Hu, S.D. Wang, Composites of metal-organic frameworks and carbon-based materials: preparations, functionalities and applications, J. Mater. Chem. A., 4 (2016) 3584–3616.
[16] N.L. Torad, M. Hu, S. Ishihara, H. Sukegawa, A.A. Belik, M. Imura, K. Ariga, Y. Sakka, Y. Yamauchi, Direct synthesis of MOF-derived nanoporous carbon with magnetic Co nanoparticles toward efficient water treatment, Small., 10 (2014) 2096–2107.
[17] X.X. Yue, W.L. Guo, X.H. Li, H.H. Zhou, R.Q. Wang, Core-shell Fe_3O_4@MIL-101(Fe) composites as heterogeneous catalysts of persulfate activation for the removal of Acid Orange 7, Environ. Sci. Pollut. Res., 23 (2016) 15218–15226.
[18] H. Motegi, K. Yano, N. Setoyama, Y. Matsuoka, T. Ohmura, A. Usuki, A facile synthesis of UiO-66 systems and their hydrothermal stability, J. Porous. Mat., 24 (2017) 1327–1333.
[19] S.K. Wu, X.P. Shen, H. Zhou, G.X. Zhu, R.Y. Wang, Z.Y. Ji, K.M. Chen, C.J. Chen, Morphological synthesis of Prussian blue analogue $Zn_3[Fe(CN)_6]_2{\cdot}xH_2O$ micro-/nanocrystals and their excellent adsorption performance toward methylene blue, J. Colloid Interface Sci., 464 (2016) 191–197.
[20] M.R. Azhar, H.R. Abid, H.Q. Sun, V. Periasamy, M.O. Tadé, S.B. Wang, One-pot synthesis of binary metal organic frameworks (HKUST-1 and UiO-66) for enhanced adsorptive removal of water contaminants, J. Colloid Interface Sci., 490 (2017) 685–694.
[21] J.R. Li, R.J. Kuppler, H.C. Zhou, Selective gas adsorption and separation in metal-organic frameworks, Chem. Soc. Rev., 38 (2009) 1477–1504.
[22] Y.B. Huang, J. Liang, X.S. Wang, R. Cao, Multifunctional metal-organic framework catalysts: synergistic catalysis and tandem reactions, Chem. Soc. Rev., 46 (2017) 126–157.
[23] Z.C. Hu, B. Deibert, J. Li, Luminescent metal-organic frameworks for chemical sensing and explosive detection, Chem. Soc. Rev., 43 (2014) 5815–5840.
[24] L. Shi, L.P. Hu, J. Zheng, M. Zhang, J.L. Xu, Adsorptive removal of methylene blue from aqueous solution using a Ni-metal organic framework material, J. Disper. Sci. Technol., 37 (2016) 1226–1231.
[25] J.J. Du, Y.P. Yuan, J.X. Sun, F.M. Peng, X. Jiang, L.G. Qiu, A.J. Xie, Y.H. Shen, J.F. Zhu, New photocatalysts based on MIL-53 metal-organic frameworks for the decolorization of methylene blue dye, J. Hazard. Mater., 190 (2011) 945–951.
[26] M.R. Azhar, H.R. Abid, V. Periasamy, H.Q. Sun, M.O. Tade, S.B. Wang, Adsorptive removal of antibiotic sulfonamide by UiO-66 and ZIF-67 for wastewater treatment, J. Colloid Interface Sci., 500 (2017) 88–95.
[27] N.A. Khan, Z. Hasan, S.H. Jhung, Adsorptive removal of hazardous materials using metal-organic frameworks (MOFs): A review, J. Hazard. Mater., 244–245 (2013) 444–456.
[28] G. Férey, C. Mellot-Draznieks, C. Serre, F. Millange, Crystallized frameworks with giant pores: are there limits to the possible, Acc. Chem. Res., 38 (2005) 217–225.
[29] H. Wang, X.Z. Yuan, Y. Wu, G.M. Zeng, X.H. Chen, L.J. Leng, H. Li, Synthesis and applications of novel graphitic carbon nitride/metal-organic frameworks mesoporous photocatalyst for dyes removal, Appl. Catal. B-Environ., 174–175 (2015) 445–454.
[30] S.H. Huo, X.P. Yan, Metal-organic framework MIL-100(Fe) for the adsorption of malachite green from aqueous solution, J. Mater. Chem., 22 (2012) 7449–7455.
[31] E. Haque, J.E. Lee, I.T. Jang, Y.K. Hwang, J.S. Chang, J. Jegal, S.H. Jhung, Adsorptive removal of methyl orange from aqueous solution with metal-organic frameworks, porous chromium-benzene dicarboxylates, J. Hazard. Mater., 181 (2010) 535–542.
[32] M.M. Zhou, Y.N. Wu, J.L. Qiao, J. Zhang, A. McDonald, G.T. Li, F.T. Li, The removal of bisphenol A from aqueous solutions by MIL-53(Al) and mesostructured MIL-53(Al), J. Colloid Interface Sci., 405 (2013) 157–163.

[33] A. Boutin, S. Couck, F.X. Coudert, P. Serra-Crespo, J. Gascon, F. Kapteijn, A.H. Fuchs, J.F.M. Denayer, Thermodynamic analysis of the breathing of amino-functionalized MIL-53(Al) upon CO_2 adsorption, Micropor. Mesopor. Mater., 140 (2011) 108–113.
[34] S. Couck, E. Gobechiya, C.E.A. Kirschhock, P. Serra-Crespo, J. Juan-Alcañiz, A. MartinezJoaristi, E. Stavitski, J. Gascon, F. Kapteijn, G.V. Baron, J.F.M. Denayer, Adsorption and separation of light gases on an amino-functionalized metal-organic framework: an adsorption and in situ XRD study, Chem. Sus. Chem., 5 (2012) 740–750.
[35] K.L. Ai, Y.L. Liu, C.P. Ruan, L.H. Lu, G.Q. Lu, Sp^2 C-dominant N-doped carbon sub-micrometer spheres with a tunable size: a versatile platform for highly efficient oxygen-reduction catalysts, Adv. Mater., 25 (2013) 998–1003.
[36] B.Q. Mao, Q.D. An, Z.Y. Xiao, S.R. Zhai, Hydrophilic hollow Fe_3O_4@PDA spheres with a storage cavity for efficient removal of polycyclic structured tetracycline, New J. Chem., 41 (2017) 1235–1244.
[37] Z.H. Dong, D. Wang, X. Liu, X.F. Pei, L.W. Chen, J. Jin, Bio-inspired surface-functionalization of graphene oxide for the adsorption of organic dyes and heavy metal ions with a superhigh capacity, J. Mater. Chem. A, 2 (2014) 5034–5040.
[38] Z.W. Zhou, R. Liu, Fe_3O_4@polydopamine and derived Fe_3O_4@ carbon core-shell nanoparticles: Comparison in adsorption for cationic and anionic dyes, Colloids and Surfaces A: Physicochem. Eng. Asp., 522 (2017) 260–265.
[39] B. Seoane, C. Téllez, J. Coronas, C. Staudt, NH_2-MIL-53(Al) and NH_2-MIL-101(Al) in sulfur-containing copolyimide mixed matrix membranes for gas separation, Sep. Purif. Technol., 111 (2013) 72–81.
[40] Y.F. Yang, W.J. Wang, H. Li, X.G. Jin, H.F. Wang, L. Zhang, Y. Zhang, NH_2-MIL-53(Al) nanocrystals anchored on the surface of RGO hollow spheres and its visible light degradation of methylene blue, Mater Lett., 197 (2017) 17–20.
[41] T. Ahnfeldt, D. Gunzelmann, T. Loiseau, D. Hirsemann, J. Senker, G. Férey, N. Stock, Synthesis and modification of a functionalized 3D open-framework structure with MIL-53 topology, Inorg. Chem., 48 (2009) 3057–3064.
[42] X.Q. Cheng, A.F. Zhang, K.K. Hou, M. Liu, Y. Wang, C. Song, G. Zhang, X. Guo, Size- and morphology-controlled NH_2-MIL-53(Al) prepared in DMF-water mixed solvents, Dalton Trans., 42 (2013) 13698–13705.
[43] C. Li, Z.H. Xiong, J.M. Zhang, C.S. Wu, The strengthening role of the amino group in metal-organic framework MIL-53(Al) for methylene blue and malachite green dye adsorption, J. Chem. Eng. Data., 60 (2015) A–I.
[44] W.J. Liu, C. Yao, M.H. Wang, J.L. Ji, L. Ying, C.Y. Fu, Kinetics and thermodynamics characteristics of cationic yellow X-GL adsorption on /ricehull-based activated carbon nanocomposite, Environ. Prog. Sustain., 32 (2013) 655–662.
[45] M.T. Yagub, T.K. Sen, S. Afroze, H.M. Ang, Dye and its removal from aqueous solution by adsorption: A review, Adv. Colloid Interface Sci., 209 (2014) 172–184.
[46] R.J. Goldacre, J.N. Philips, The ionization of basic triphenylmethane dyes, J. Chem. Soc., (1949) 1724–1732.
[47] H.C. Liu, L.G. Chen, J. Ding, Adsorption behavior of magnetic amino-functionalized metal-organic framework for cationic and anionic dyes from aqueous solution, RSC Adv., 6 (2016) 48884–48895.
[48] Q.Y. Xie, Y. Li, Z.L. Lv, H. Zhou, X.J. Yang, J. Chen, H. Guo, Effective adsorption and removal of phosphate from aqueous solutions and eutrophic water by Fe-based MOFs of MIL-101, Sci. Rep., 7 (2017) 1–15.
[49] Z. Hasan, E.J. Choi, S.H. Jhung, Adsorption of naproxen and clofibric acid over a metal-organic framework MIL-101 functionalized with acidic and basic groups, Chem. Eng. J., 219 (2013) 537–544.
[50] S. Dadfarnia, A.M. Haji Shabani, S.E. Moradi, S. Emami, Methyl red removal from water by iron based metal-organic frameworks loaded onto iron oxide nanoparticle adsorbent, Appl. Surf. Sci., 330 (2015) 85–93.
[51] M.K. Purkait, S. DasGupta, S. De, Determination of thermodynamic parameters for the cloud point extraction of different dyes using TX-100 and TX-114, Desalination, 244 (2009) 130–138.
[52] X. Ren, Z. Xiong, Adsorption behavior of three nitroimidazoles in aqueous solutions to magnetic-modified multi-walled carbon nanotubes, Acta Chimica Sinica., 71 (2013) 625–633.
[53] J.W. Fu, Z.H. Chen, M.H. Wang, S.J. Liu, J.H. Zhang, J.N. Zhang, R.P. Han, Q. Xu, Adsorption of methylene blue by a high-efficiency adsorbent (polydopamine microspheres): kinetics, isotherm, thermodynamics and mechanism analysis, Chem. Eng. J., 259 (2015) 53–61.
[54] B. Liu, F. Yang, Y. Zou, Y. Peng, Adsorption of phenol and p-nitrophenol from aqueous solutions on metal-organic frameworks: effect of hydrogen bonding, J. Chem. Eng. Data., 59 (2014) 1476–1482.